Structural Properties of Lead Oxide-Doped Zinc Tellurite Glasses

Hiwa L. Hamad*, Saman Q. Mawlud

Department of physics, College of Education, Salahaddin University-Erbil, Kurdistan Region, Iraq

ABSTRACT

The melt quenching technique was used to create a ternary $(90-x)$ TeO_2 - $xPbO$ - $10ZnO$ glass system (x = 0, 10, 20, 25, 30, 35, and 40 mol%). The X-ray diffraction (XRD) technique is used for improving the amorphous nature of the glass samples. In addition, to examine the structural characteristics of the glass samples, scanning electron microscopy (SEM) and energy dispersive X-ray (EDX) spectroscopy are used. Raman spectroscopy was used to evaluate the impact of PbO on the glass structure. A strong frequency peak at 729.63-774.69 cm^{-1} was detected in the Raman spectra, indicating that the TeO_4 and TeO_3/TeO_{3+1} structural units make up the majority of the glass network. The TeO_3/TeO_{3+1} structural unit contain non-bonding oxygen molecules that are stretched in the Pb-O, Zn-O, Te-O, and Te-O-Te bridging configurations, vibrations, and Raman spectra.

1.Introduction

Tellurite oxide (TeO$_2$) based glasses have a number of important features that make them of interest in science and technology, including good transparency in the visible and infrared areas (0.4–6 μm), high dielectric constants, high refractive indices, and low melting temperatures(El-Mallawany, 2001). TeO2 is a member of the intermediate class of glass-forming oxides because, according to a study (Narayanan and Zwanziger, 2003, Suehara et al., 1995), it cannot produce glass on its own without the addition of metal oxides like Na2O, BaO, PbO, ZnO, or Nb2O5. By producing structural unit alterations, breaking structural unit chains, and raising entropy, modifier molecules in glass forming often improve the glass formation ability (GFA)(Mawlud et al., 2016b, Kaur et al., 2010).

Tellurite glasses are used in a wide variety of applications, They are used in gas sensors, ultra-broadband fiber Raman amplifiers, and infrared to visible light conversion (Balda et al., 2007, Mawlud and Beyond, 2018). Glasses made of heavy metal oxides are excellent candidates for stimulated Raman scattering (SRS)-based delayed light production (Qin et al., 2007). In non-linear optics for second and third-harmonic generation, tellurite glasses, especially zinc and lead tellurite, are of interest (Souza et al., 2006, Narazaki et al., 1999).

The trigonal bipyramid TeO$_4$, deformed TeO$_4$, TeO$_{3+1}$ polyhedron, and trigonal TeO$_3$ structural units make up the structure of TeO$_2$ to be rich among the other glasses. Each TeO$_4$ unit has two Te-O$_{ax}$ bonds, which are very mobile and are easily affected by network modifier atoms. One of the Te-O$_{ax}$ links in TeO$_4$ polyhedral gets wider, the bond length rises from 0.208 to 0.298 nm, and a TeO3+1 structural unit is created when a network modifier such as metal oxide is introduced to the glass matrix. TeO$_4$ transforms into a TeO$_3$ structural unit when the length of the Te-O link reaches 0.298 nm (Singh and Chakravarthi, 1997). Normally referred to as structural units TeO$_4$, TeO$_{3+1}$, and TeO$_3$ namely Q_4^4 ,Q_4^3 and $Q_3^{2,1,0}$, respectively (McLaughlin et al., 2000, Narayanan and Zwanziger, 2003,

Ahmed et al., 2017a). Thus, the superscript is the quantity of bridging oxygen connected to a Te atom, and the subscript is the number of oxygen that is coordinated around the Te atom.

The aim of this research is to prepare a series of glass with the chemical composition of (90-x) TeO$_2$ - xPbO -10ZnO (x = 0, 10, 20, 25, 30, 35, and 40 mol %) by using the melt-quenching method and then characterizing the glass to study the structural properties with the aid of XRD, EDX, and Raman scattering measurements.

2. Experimental Part

A series of lead zinc tellurite glasses are prepared using the melt quenching method from chemically pure raw materials, with a composition of (90-x) TeO$_2$ - xPbO -10ZnO (x=0, 10, 20, 25, 30, 35, and 40 mol%). The materials used in this research

are tellurium oxide TeO$_2$ (≥99%) Sigma-Aldrich, lead oxide PbO (≥99 %) Carl Roth and zinc oxide ZnO (99.9%) Sigma-Aldrich. All the materials were in fine powder form. The corresponding 10 gm weights of the initial ingredients are thoroughly mixed to get a homogenous composition and after that, they are put in an alumina crucible, then the mixed powder with the crucible is transferred to inside an electric furnace for the melting process at 850°C for 20 minutes. After the desired viscosity of the molten is achieved, the melt is poured onto a brass mold and annealed at 280°C for one hour. Finally, the furnace is switched off and cooled down until reaches room temperature.

All the prepared glasses were cut using a diamond cutter and polished using different hardness degrees of sandpaper of various grits from 120 to 1200 to produce a clean and smooth surface for the glass samples as shown in figure 1. The estimated average thickness of the glass samples was around 3 mm. X-Ray diffraction (XRD) (Panalytical X' Pert Pro) in the range 5° to 80° is used to verify the amorphous structure, energy dispersive EDX (Oxford Instrument A-Z tech) and Scanning Electron Microscopy FESEM (ZEIS SIGMA VP) analysis used for studying the ratio of each of the chemical elements and to get the data about the morphology of the sample.

Raman spectroscopy (Horiba XploRA PLUS) with the excitation wavelength 532 nm and in the wavenumber range 50-1500 cm^{-1} is used for studying the fingerprint of the glass structure.

Figure 1: The glass samples with series (90-x) TeO$_2$ -10ZnO- xPbO

3. Results and Discussions

3.1 X-Ray Diffraction

The amorphous nature of the prepared glass samples was investigated using XRD analysis. The typical XRD patterns for the composition of (90-x) TeO$_2$ - xPbO -10ZnO (x = 0, 10, 20, 25, 30, 35, and 40 mol %) are depicted in Figures 2. The amorphous character of the produced glasses is confirmed by the existence of a wide hump between 25° and 35° without any sharp crystallization peaks (Saudi et al., 2021, MAWLUD, 2016, Ahmed et al., 2017a). The presence of long-range structural disorder in the prepared glasses is illustrated by the broad dispersed scattering at lower angles. Similar result for the XRD pattern is observed by other previously published research (Yusof et al., 2017, Mawlud et al., 2017b).
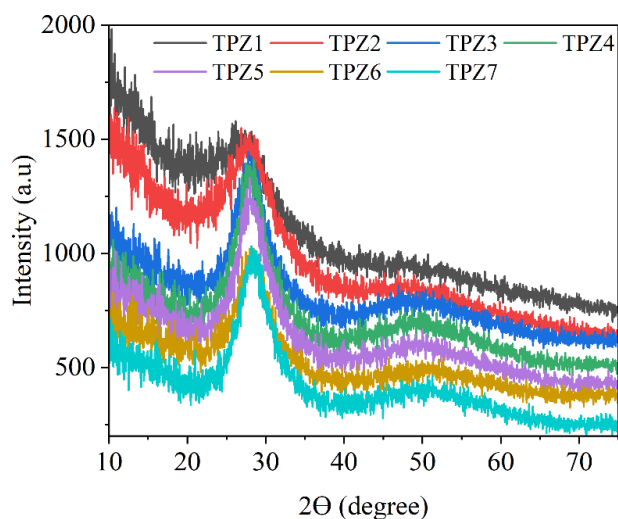
Figure 2: Typical XRD pattern of glass with series (90-x) TeO$_2$ -10ZnO- xPbO

3.2 EDX Spectra and SEM Micrograph

The EDX spectrum measures the concentration of each element in the glasses. It is important to understand that EDX measures elements by finding out the area beneath the peak of each one that is found (Mawlud et al., 2017a). The 60TeO$_2$-30PbO-10ZnO glass sample was placed for SEM-EDX analyses to look for both morphological and chemical alterations. The elements such as, Te, O, Pb, and Zn appear in the usual EDX spectrum of a TPZ5 glass sample from the selected area, as shown in Figure 3. These elements are ascribed to traces of elemental material in the glass matrix nearby. The detection of components verifies that the necessary glass samples were successfully prepared. Table 1 provides a quantitative examination of the EDX spectra for all the prepared glass samples. It demonstrates the elements' atomic and weight percentages. The appearance of the carbon peak is related to the vacuum-evaporated carbon from the coating material and from the carbon tape that was used for adjusting the sample on the sample holder. Usually, samples are frequently electrically non-conducting, necessitating the application of a conducting surface coating to create a pathway for incoming electrons to travel to ground. In this case, the powder sample needs to be coated with the gold by using the sputtering technique in order to minimize the process and thus the strong peak of gold will appear in the EDX spectra. Therefore, there are differences between the estimated and observed percentages of the elements (wt. %). These differences result from EDX studies, which

calculate the area under the peak of each detected component to estimate the components (Fultz and Howe, 2012, Mawlud et al., 2017b). All TeO$_2$-PbO-ZnO glass samples under investigation provided findings that were identical.
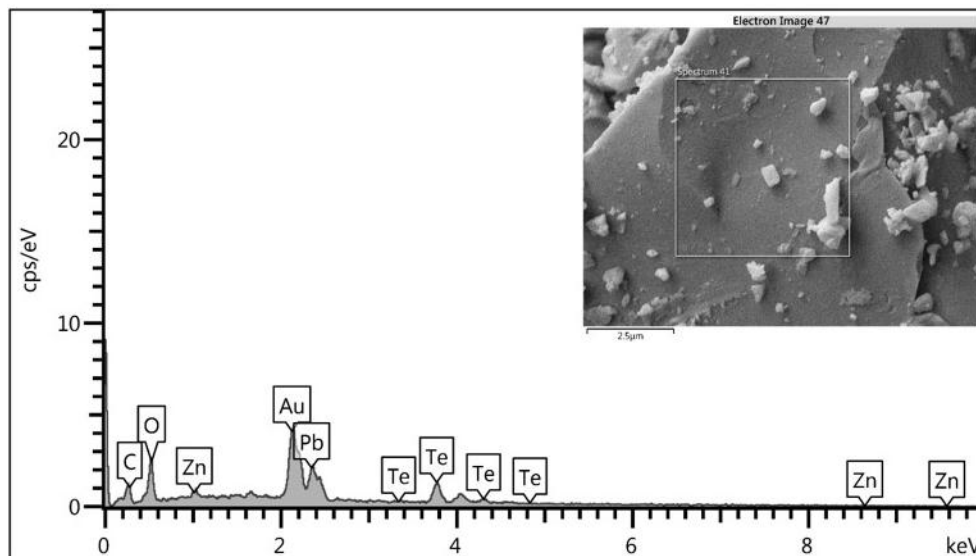
Figure 3: Finding of microstructure and EDX/SEM analysis of 60TeO$_2$-30PbO-10ZnO (TPZ5) glass sample

The SEM micrographs of the glass samples, which Display in Figure 4, demonstrates the asymmetrical grain and various rod-type structures. SEM micrographs for all the glass samples have shown a homogeneous glassy phase (Mawlud et al., 2017b). Both dimensions show an irregular shape of grains and this structure can be observed for other glass samples. This confirmed the homogeneous and amorphous nature of the prepared glasses (Pal et al., 2012)

Table 1: Calculated and EDX-measured element weight for all glass samples TPZ.

Glass code	Oxygen		Lead		Tellurite		Zinc	
	Experimental Weight %	Calculated Weight %	Experimental Weight %	Calculated Weight %	Experimental Weight %	Calculated Weight %	Experimental Weight %	Calculated Weight %
TPZ1	8.7	20.01	0	0	89.2	75.67	1	4.30
TPZ2	8.3	18.20	13.9	13.10	74.7	64.55	3.1	4.12
TPZ3	7.1	16.52	36	25.19	52.2	54.30	1.2	3.97
TPZ4	6.4	15.71	35.7	30.89	52.2	49.46	1.2	3.89
TPZ5	6.9	14.97	38.2	36.38	47.8	44.81	2.4	3.82
TPZ6	6.2	14.24	38.1	41.67	48.7	40.32	2.8	3.75
TPZ7	5.4	15.71	41.2	46.35	46.4	35.68	4.2	3.65
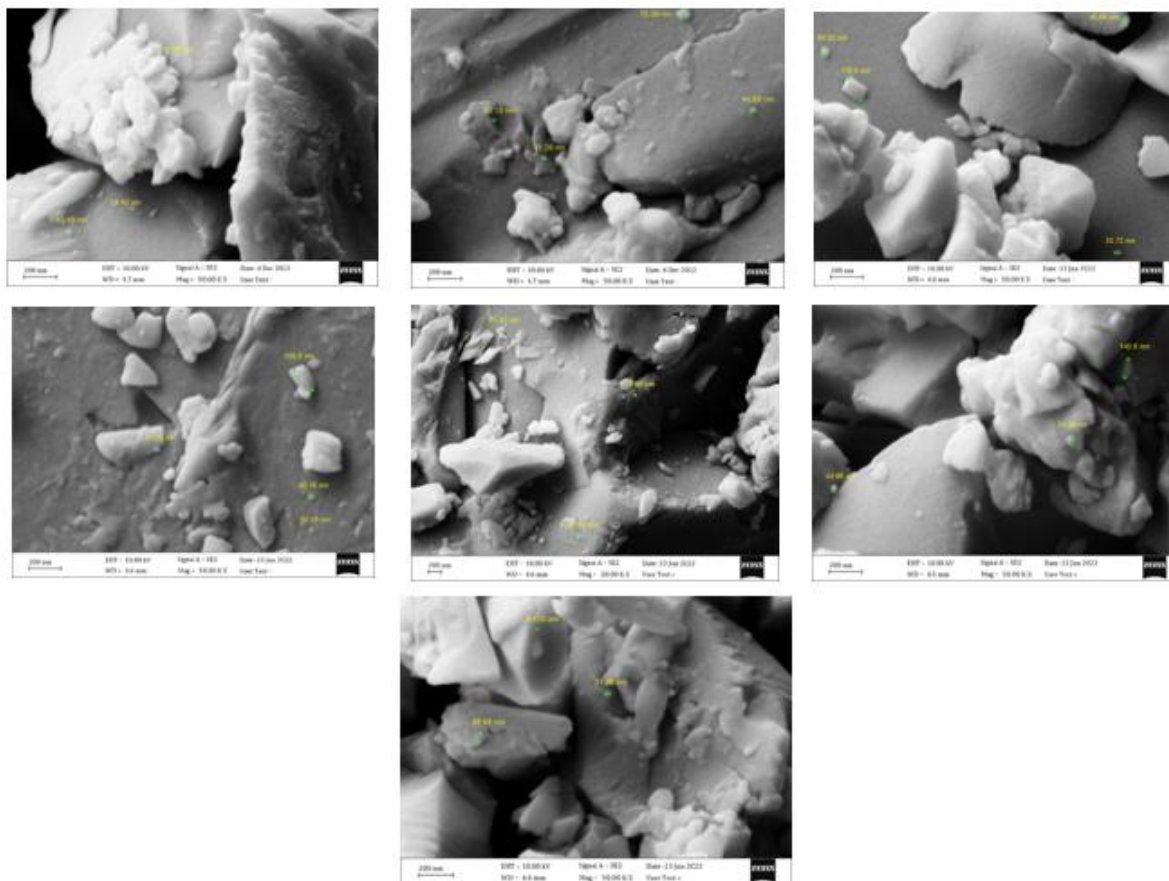
Figure 4: Scanning electron microscope (SEM) of all the prepared glass samples TPZ.

3.3 Raman Spectroscopy

Raman spectroscopy is one of the most well-known varieties of vibrational spectroscopy. It is regarded as a fingerprint containing glass's structural data. Figure 4 depicts the TPZ glass series' Raman spectra in the frequency range of 100-900 cm^{-1}. The total of these selections is shown by a dotted line that closely matches the solid line derived from the Raman spectra. These peaks are concentrated at 335.47, 449.29, 670.72, and 734.19 cm^{-1} which are denoted by (A, B, C, and D) respectively. The observed peaks are appropriate with previous results that has been done(Mawlud et al., 2016a).

The relevant absorption peak shifts are listed in Table 2. All band areas between 318.87-346.23 cm^{-1}, 449.29-463.52 cm^{-1}, 661.24-675.46 cm^{-1}, and 729.63-774.69 cm^{-1} could be shown to be dominate in the shift. Both PbO and TeO$_3$ tp may be attributed to the Raman band in the range of 318.87 and 346.23 cm^{-1}, indicating that the presence of heavy metals may considerably alter the Te-O networking structure in the glass samples. Te-O-Te links vibration is the cause of the Raman shift related to the band in the region of 449.29-463.52 cm^{-1}. At the same time, the Raman peaks shift in the range of 661.24-675.46 cm^{-1} and 729.63-774.69 cm^{-1}, which correspond to TeO$_3$ bp unit and TeO$_4$ tbp unit, respectively (Ticha et al., 2019, Ahmed et al., 2017b).

The one broad and extremely asymmetrical peak in the wavenumber of the BO motion may be divided at least into two peaks, with its form drastically shifting with changes in the chemical composition (see Figure. 5). As the earlier study was observed (Ticha et al., 2017), it possible relate the lower frequency broad peaks between 318.87-346.23 cm^{-1} to the bending motion of oxygen in the Pb-O-Te and Zn-O-Te bridges. The higher frequency peak between 449.29-463.52 cm^{-1} can be attributed to the oxygen's bending motion in the Te-O-Te bridge (Ticha et al., 2019). In addition to replacing ZnO with PbO, the creation of Pb-O-Te bridges is followed by a drop in the density of Te-O-Te

bridges. In order to create NBO units, in this case, TeO_3 trigonal pyramids, a drop in the density of Te-O-Te bridges is expected, which also indicates a decrease in total network connection (Jaba et al., 2005).

In addition, as illustrated in Figure 5, it could be observed that the concentration of PbO increases the strength of the Raman peaks around 661.24-675.46 cm^{-1} and peaks about 729.63-774.69 cm^{-1}. The shift in intensity may be caused by the TeO_4 being disturbed, which results in the formation of a TeO_3 tp unit. It is claimed that adding PbO to TPZ glasses increases the amount of TeO_3 tp units produced (Table 2)(Ticha et al., 2017)

Table 2: Raman peaks position in cm^{-1} for (90-x) TeO_2 -10ZnO- xPbO

Sample code	%PbO	Raman shifts / cm^{-1}			
		A	B	C	D
TPZ1	0	335.47	455.67	665.98	774.69
TPZ2	10	337.84	450.93	668.35	758.09
TPZ3	20	330.73	463.52	661.24	729.63
TPZ4	25	340.21	451.63	675.46	734.38
TPZ5	30	335.47	449.29	670.72	734.19
TPZ6	35	318.87	461.14	673.09	741.31
TPZ7	40	346.23	449.29	665.98	738.94
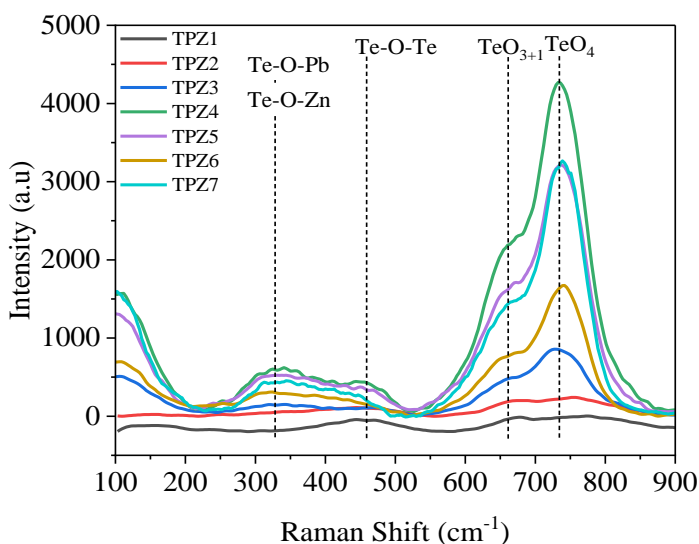
Figure 5: Raman spectra of 60TeO$_2$-30PbO-

4. Conclusions

In this work, the melt quenching technique is used to prepare the glass formation range of the (90-x) TeO_2-xPbO-10ZnO system. All samples are found to be amorphous according to the XRD data. Glass EDX maps showed that the traced elements were distributed uniformly across the host matrix. Raman spectroscopies are used to examine structural characteristics. The glass system's vibrational spectra indicated that the TeO_4, TeO_3/TeO_{3+1}, PbO, and ZnO units make up the glass network. According to Raman scattering investigations, adding the glass modifier PbO mol% causes a shift in the relative intensities and frequencies of Raman bands. This clearly shows that the symmetry of TeO_4 bipyramidal trigonal units is continuously distorted toward the formation of TeO_3 trigonal units or the TeO_{3+1} polyhedron.

Potential conflicts of interest. All authors report no conflicts of interest relevant to this article.

References

Ahmed, K. F., Ibrahim, S. O., Sahar, M. R., Mawlud, S. Q. & Khizir, H. A. Thermal analyses, spectral characterization and structural interpretation of Nd3+/Er3+ ions co-doped TeO2-ZnCl2 glasses system. AIP Conference Proceedings, 2017a. AIP Publishing LLC, 020008.

Ahmed, K. F., Ibrahim, S. O., Sahar, M. R., Mawlud, S. Q. J. Z. J. O. P. & Sciences, A. 2017b. Effect of Rare Earth Co-Doping On Physical and Optical Characterization of Zinc Tellurite Glass Embedded Ag NPs. 28, 68-73.

Balda, R., Fernández, J., Arriandiaga, M. & Fernández-Navarro, J. M. J. J. O. P. C. M. 2007. Spectroscopy and frequency upconversion in Nd3+-doped TeO2–TiO2–Nb2O5 glass. 19, 086223.

El-Mallawany, R. A. 2001. *Tellurite glasses handbook: physical properties and data*, CRC press.

Fultz, B. & Howe, J. M. 2012. *Transmission electron microscopy and diffractometry of materials*, Springer Science & Business Media.

Jaba, N., Mermet, A., Duval, E. & Champagnon, B. J. J. O. N.-C. S. 2005. Raman spectroscopy studies of Er3+-doped zinc tellurite glasses. 351, 833-837.

Kaur, A., Khanna, A., Pesquera, C., González, F. & Sathe, V. J. J. O. N.-C. S. 2010. Preparation and characterization of lead and zinc tellurite glasses. 356, 864-872.

Mawlud, S. Q. Absorption and luminescence spectral properties study of Sm3+ doped TeO2-Na2O glasses. Proc. Int. Sci. Postgraduate Conf., 2016. 1-10.

Mawlud, S. Q., Ameen, M., Sahar, R. M. & Ahmed, K. J. J. a. M. E. 2016a. Infiuence of Sm2O3 ion concentration on structural and thermal modification of TeO2-Na2O glasses. 5.

Mawlud, S. Q., Ameen, M. M., Sahar, M. R. & Ahmed, K. F. J. J. O. L. 2017a. Plasmon-enhanced luminescence of samarium doped sodium tellurite glasses embedded with gold nanoparticles: Judd-Ofelt parameter. 190, 468-475.

Mawlud, S. Q., Ameen, M. M., Sahar, M. R., Ahmed, K. F. J. S. S. S. & Technology. 2016b. Optical absorption spectra of samarium doped TeO2-Na2O glasses. 24, 94-106.

Mawlud, S. Q., Ameen, M. M., Sahar, R. B., Ahmed, K. F. J. Z. J. O. P. & Sciences, A. 2017b. Structural and thermal behavior of Sm3+ ions doped sodium tellutite glasses. 29.

Mawlud, S. Q. J. T. G. S. M. a. I. O. & Beyond. 2018. Optical Properties of Tellurite Glasses Embedded with Gold Nanoparticles. 105-142.

Mclaughlin, J., Tagg, S., Zwanziger, J., Haeffner, D. & Shastri, S. J. J. O. N.-C. S. 2000. The structure of tellurite glass: a combined NMR, neutron diffraction, and X-ray diffraction study. 274, 1-8.

Narayanan, R. A. & Zwanziger, J. W. J. J. O. N.-C. S. 2003. The glass forming ability of tellurites: a rigid polytope approach. 316, 273-280.

Narazaki, A., Tanaka, K., Hirao, K. & Soga, N. J. J. O. a. P. 1999. Induction and relaxation of optical second-order nonlinearity in tellurite glasses. 85, 2046-2051.

Pal, I., Agarwal, A., Sanghi, S. & Aggarwal, M. J. O. M. 2012. Structure and optical absorption of Sm3+ and Nd3+ ions in cadmium bismuth borate glasses with large radiative transition probabilities. 34, 1171-1180.

Qin, G., Jose, R. & Ohishi, Y. J. J. O. a. P. 2007. Stimulated Raman scattering in tellurite glasses as a potential system for slow light generation. 101, 093109.

Saudi, H., Tekin, H., Zakaly, H. M., Issa, S. A., Susoy, G. & Zhukovsky, M. J. O. M. 2021. The impact of samarium (III) oxide on structural, optical and radiation shielding properties of thallium-borate glasses: Experimental and numerical investigation. 114, 110948.

Singh, R. & Chakravarthi, J. J. P. R. B. 1997. dc conductivity of V 2 O 5-containing zinc tellurite glasses. 55, 5550.

Souza, R. F., Alencar, M. A., Hickmann, J. M., Kobayashi, R. & Kassab, L. R. J. a. P. L. 2006. Femtosecond nonlinear optical properties of tellurite glasses. 89, 171917.

Suehara, S., Yamamoto, K., Hishita, S., Aizawa, T., Inoue, S. & Nukui, A. J. P. R. B. 1995. Bonding nature in tellurite glasses. 51, 14919.

Ticha, H., Schwarz, J. & Tichy, L. J. J. O. N.-C. S. 2017. On the structural arrangement and optical band gap (PbO) x (ZnO) 10 (TeO2) 90− x glasses. 459, 63-67.

Ticha, H., Schwarz, J., Tichy, L. J. M. C. & Physics. 2019. Raman spectra and optical band gap in some PbO-ZnO-TeO2 glasses. 237, 121834.

Yusof, N., Ghoshal, S., Azlan, M. J. J. O. A. & Compounds. 2017. Optical properties of titania nanoparticles embedded Er3+-doped tellurite glass: Judd-Ofelt analysis. 724, 1083-1092.